LETTER

doi:10.1038/nature13484

Structural basis for lipopolysaccharide insertion in the bacterial outer membrane

Shuai Qiao[1,2], Qingshan Luo[1,2], Yan Zhao[1,3], Xuejun Cai Zhang[1] & Yihua Huang[1]

One of the fundamental properties of biological membranes is the asymmetric distribution of membrane lipids. In Gram-negative bacteria, the outer leaflet of the outer membrane is composed predominantly of lipopolysaccharides (LPS)[1]. The export of LPS requires seven essential lipopolysaccharide transport (Lpt) proteins to move LPS from the inner membrane, through the periplasm to the surface[2]. Of the seven Lpt proteins, the LptD–LptE complex is responsible for inserting LPS into the external leaflet of the outer membrane[3,4]. Here we report the crystal structure of the ~110-kilodalton membrane protein complex LptD–LptE from *Shigella flexneri* at 2.4 Å resolution. The structure reveals an unprecedented two-protein plug-and-barrel architecture with LptE embedded into a 26-stranded β-barrel formed by LptD. Importantly, the secondary structures of the first two β-strands are distorted by two proline residues, weakening their interactions with neighbouring β-strands and creating a potential portal on the barrel wall that could allow lateral diffusion of LPS into the outer membrane. The crystal structure of the LptD–LptE complex opens the door to new antibiotic strategies targeting the bacterial outer membrane.

The outer membrane of Gram-negative bacteria is comprised of an asymmetric lipid bilayer with phospholipids in the inner leaflet and glycolipids, predominately lipopolysaccharide (LPS), in the outer leaflet[1]. The LPS layer in the outer membrane endows Gram-negative bacteria with a strong permeability barrier against toxic compounds such as antibiotics, allowing survival in harsh environments[5]. LPS is also a potent activator of the innate immune response and acts as a conserved pathogen-associated molecular pattern (PAMP) recognized by innate immune receptors[6]. Given its functional importance, it is not surprising that LPS is essential to most Gram-negative bacteria, and intervening in its biogenesis pathway offers great opportunities for developing novel antibiotics against pathogenic bacteria.

In *Escherichia coli*, the transport of LPS molecules from the outer leaflet of the inner membrane to the cell surface is executed by the LPS transport (Lpt) machinery[7], which consists of seven essential proteins (LptA–LptG)[2]. Once extracted from the inner membrane by an ATP-binding-cassette (ABC) transporter complex comprised of LptB, LptF and LptG[8], the detached LPS molecule is delivered to LptC[9] and further to LptA in an ATP-dependent manner[10]. The final stage of LPS transport to the cell surface is accomplished by an outer-membrane-localized two-protein complex, LptD–LptE[3,4]. However, the precise mechanism of LPS insertion and assembly in the outer membrane remains obscure. Here, we report the crystal structure of the LptD–LptE complex from *Shigella flexneri* at 2.4 Å resolution. The structure provides mechanistic insights into how LPS is exported to and inserted in the outer leaflet of the outer membrane.

One remarkable feature of the LptD–LptE complex is the observation of two pairs of non-consecutive disulphide bonds in LptD: residues Cys 31 and Cys 173 form disulphide bonds with residues Cys 724 and Cys 725, respectively, confirming previous functional analyses[11–13] (Fig. 1a, c). To validate the presence of disulphide bonds in the purified recombinant protein of LptD, we performed SDS–PAGE analysis for purified LptD–LptE complex under both reducing and non-reducing conditions. As shown in Fig. 1b, LptD exhibited slower mobility on SDS–PAGE with an apparent molecular weight of 130 kDa under non-reducing conditions, but returned to its calculated molecular weight of 87 kDa under reducing conditions, indicating the presence of disulphide bonds within LptD. The LptD–LptE complex was unable to dissociate on SDS–PAGE

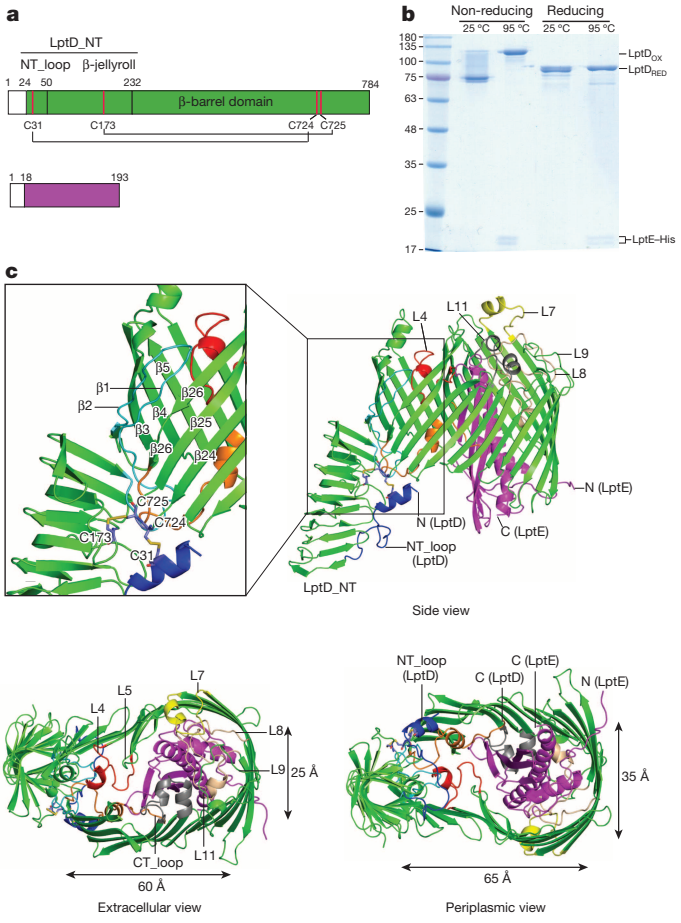

Figure 1 | General architecture of the LptD–LptE complex. **a**, Schematic structures of LptD and LptE. **b**, SDS–PAGE showing the presence of disulphide bonds within LptD and stability of the LptD–LptE complex. $LptD_{OX}$ and $LptD_{RED}$ represent the oxidized and reduced LptD, respectively. Data shown are representative of at least three independent experiments. **c**, Cartoon representation of the LptD–LptE complex. LptD and LptE are coloured in green and magenta, respectively. Strands β1 and β2 are highlighted in cyan. Extracellular loops L4, L7, L8 and L11 are coloured in red, yellow, wheat and grey, respectively. The N-terminal loop (NT_loop) and the C-terminal loop (CT_loop) of LptD are highlighted in blue and orange, respectively. Dimensions of the LptD–LptE complex are marked.

[1]National Laboratory of Biomacromolecules, National Center of Protein Science-Beijing, Institute of Biophysics, Chinese Academy of Sciences, Beijing 100101, China. [2]University of Chinese Academy of Sciences, Beijing 100101, China. [3]School of Life Sciences, University of Science and Technology of China, Hefei 230027, Anhui, China.

unless the samples were heated for 10 min at 95 °C, suggesting LptD and LptE form a tight complex (Fig. 1b). Additionally, disruption of any of the two disulphide bonds caused partial degradation of LptD and promiscuous disulphide bond formation within LptD when co-expressed with LptE (Extended Data Fig. 3).

The amino terminus of LptD (LptD_NT, residues 24–232) can be subdivided into a 26-residue fragment (NT_loop, residues 24–50) and a β-jellyroll domain (Figs 1c and 2a), confirming a previous prediction[2]. Each of the two β-sheets of the β-jellyroll consists of eleven antiparallel β-strands[14,15] (Fig. 2a). The interior surface of the β-jellyroll is highly hydrophobic with two bound detergent molecules (Fig. 2a and Extended Data Fig. 7a), indicating its role in binding the hydrophobic moiety of LPS in a manner that resembles LptA and LptC[16,17]. Structure superposition of LptD_NT with LptA and LptC showed high structural similarities between them, with an r.m.s.d. (root-mean-square deviation) of 1.7 Å (117 Cα atoms) to LptA and 2.6 Å (106 Cα atoms) to LptC, respectively (Fig. 2b, c). Previous studies showed that residues Ile 36, Phe 95 and Leu 116 of LptA bind LPS *in vivo*[10]. The high structural similarity between LptD_NT and LptA implies that corresponding residues Val 51, Tyr 112 and Leu 128 of LptD_NT may also bind LPS (Fig. 2b and Extended Data Fig. 4). The NT_loop of LptD_NT starts with a short α-helix near the β-barrel and runs in the reverse direction from that of the β-jellyroll (Figs 1c and 2a).

The carboxy terminus of LptD (residues 233–784) forms a kidney-shaped β-barrel composed of twenty-six antiparallel β-strands (termed β1–β26; Fig. 1c). The β-barrel has periplasmic and extracellular dimensions of 65 Å × 35 Å and 60 Å × 25 Å, respectively (Fig. 1c, Cα distance). Therefore, LptD is the largest single-protein β-pore observed to date. The plugging of LptE inside of the barrel causes a diminished lumen size to 45 Å × 35 Å on the periplasmic side. Given that the dimensions of Ra LPS molecule is about 32 Å × 28 Å × 12 Å (ref. 18; Extended Data Fig. 1b), the size of the vacant lumen inside of the LptD–LptE complex on the periplasmic side is sufficiently large for accommodating Ra LPS.

Strikingly, among the 26 strands that constitute the barrel, the secondary structures of the first two strands are distorted, presumably because of the presence of two proline residues at the positions of 231 and 246 (Fig. 3a). In particular, Pro 231 terminates the strand β1 at the N-terminal end. As a consequence, β1 forms only three main-chain hydrogen bonds to its neighbouring strand β26 (Fig. 3b). Likewise, Pro 246 breaks strand β2 in the middle, leaving only four and five hydrogen bonds to β1 and β3, respectively (Fig. 3b). The interaction between β1 and β2 is also mediated by an inter-strand salt bridge formed between Glu 242 and Lys 234 inside the β-barrel (Extended Data Fig. 8). Additionally, Pro 261, which is located in strand β3, may also contribute to weakened β-sheet formation with the upper portion of β2 (Fig. 3a). An alignment of LptD orthologues from 25 species revealed the conservation of proline residues, Pro 231, Pro 246 and Pro 261 (Extended Data Fig. 2).We predict that the hairpin formed by strands β1 and β2 may function as a door, creating a gate with a width as large as 16 Å between strands β3 and β26 upon dislocation (Fig. 3a). Consistent with this hypothesis, the average B-factors for both β1 and upper portion of β2 (36.8 $Å^2$ for Cα atoms of residues 228–249) are much higher than those of other β-strands (21.0 $Å^2$ for Cα atoms of residues 255–757) that constitute the rest of the β-barrel, indicating that this portion is more dynamic in the membrane. Intriguingly, side chains of four aromatic residues (Tyr 235, Phe 241, Tyr 244 and Phe 754) adopt alternating conformations and are all located at the potential LPS exit portal (Fig. 3a and Extended Data Fig. 7b). It is likely that these aromatic residues may play certain roles in LPS export into the outer membrane.

Unlike the highly hydrophobic nature of the interiors of LptA, LptC, LptD_NT and MD-2, which all bind the hydrophobic moiety of LPS[14,15,18], the interior of the LptD–LptE complex is fairly hydrophilic (Extended Data Fig. 5). The charged residues do not form clusters but are uniformly distributed inside the barrel, suggesting that the entry of the hydrophobic moiety of LPS to the barrel is energetically unfavourable, but this inner surface property may favour the hydrophilic moiety of

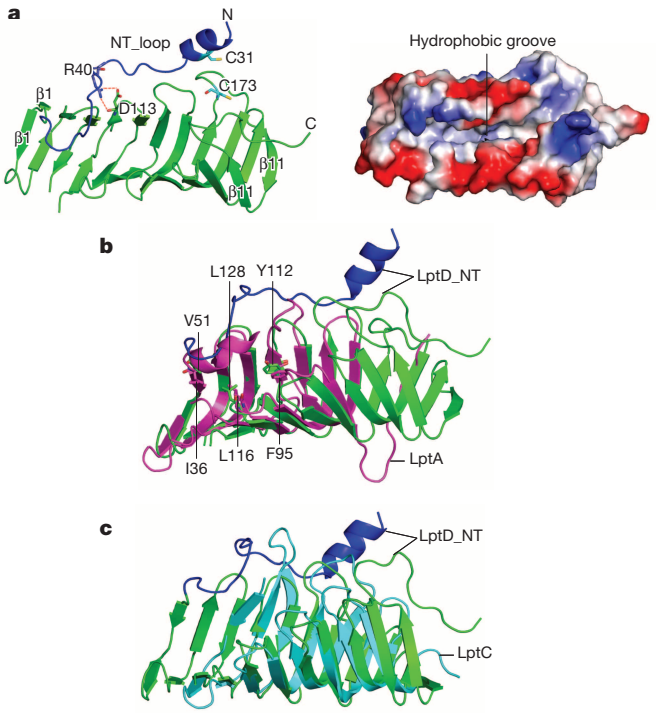

Figure 2 | The N terminus of LptD (LptD_NT) forms a β-jellyroll that functions in LPS transport. **a**, Cartoon and electrostatic surface representation of LptD_NT. LptD_NT contains an NT_loop (blue) and a β-jellyroll (green). Surface representation of the electrostatic potential (right) shows the hydrophobic interior of the β-jellyroll. For clarity, the NT_loop is omitted. **b**, Superposition of LptD_NT (green) with LptA (magenta) showing the structural similarities. Residues V51, Y112 and L128 of LptD_NT may bind the fatty acyl chains of LPS. **c**, Superposition of LptD_NT (green) with LptC (cyan).

LPS entry into the barrel of the LptD–LptE complex. Consistent with this hypothesis, there is a large hole at the interface between LptD_NT and the LptD barrel, and a portion of LptD_NT may reside into the lipid phase of the outer membrane (Figs 1c, 3a and Extended Data Fig. 5a).

LptE has three distinct functions, namely LptD assembly, LptD plugging, and LPS export[19–22]. In the current crystal structure, the N terminus of LptE seems to be located at a place corresponding to the inner leaflet of the outer membrane (Fig. 1c), although the *N*-acyl-*S*-diacylglycerylcysteine moiety is invisible in the structure. LptE adopts an α/β structure, in which five β-strands form the potential LPS-binding surface (Fig. 4a). Despite low sequence identity, the structure of LptD-bound LptE from *S. flexneri* highly resembles its orthologues from *Shewanella oneidensis* (PDB ID 2R76), *Nitrosomonas europaea* (PDB ID 2JXP) and *Neisseria meningitides* (PDB ID 3BF2), with an r.m.s.d. of 1.7 Å (127 Cα atoms), 2.4 Å (133 Cα atoms), 1.7 Å (115 Cα atoms), respectively (Extended Data Fig. 6)[22]. Surface electrostatic potential of LptE reveals that hydrophobic and hydrophilic patches are evenly distributed on the potential LPS-interacting surface (Fig. 4a), indicating that it is unlikely that the highly hydrophobic moiety of LPS bind to LptE[14,15,18]. Given the chemical composition of LPS, LptE may bind to the polar head of lipid A that consists of phosphate groups and two glucosamine units (Extended Data Fig. 1)[20].

The interaction between LptD and LptE buries a surface area of 6,500 $Å^2$ from both proteins in the complex. Apart from a hydrophobic cluster that is contributed by residues Val 89 and Phe 90 from LptE and residues Ile 664, Ile 682, Tyr 678, Ile 736, Ile 777 and Ile 778 from LptD, residues from L4 and L8 of LptD, residues from the CT_loop of LptD and residues from the inner wall of LptD β-barrel make extensive polar interactions to LptE (Fig. 4b, c). It was shown in ref. 22 that LptD residues 529–538 are in close contact with LptE, and disrupting this interaction

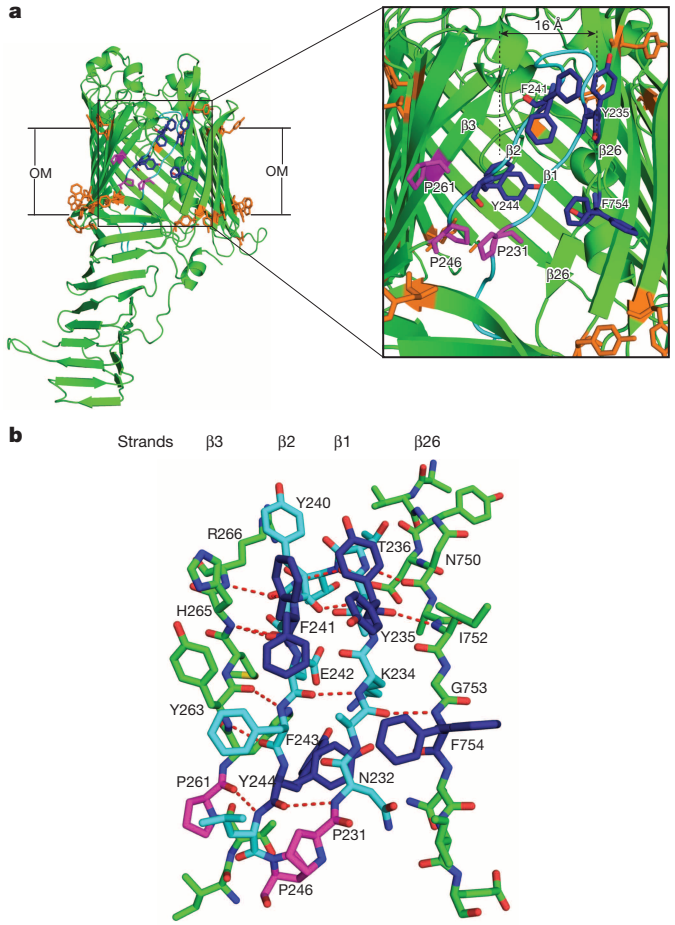

Figure 3 | Features of the LPS exit portal on the LptD barrel wall. **a**, Cartoon representation of LptD showing the potential LPS exit portal on the barrel wall (for clarity, LptE is omitted). The aromatic residue-belts (orange) delineate the membrane-solvent boundaries. Important proline residues P231, P246 and P261 are labelled and shown in stick mode. Side chains of residues (Y235, F241, Y244 and F754) adopt alternating conformations (blue). The potential LPS exit portal has an approximate width of 16 Å. **b**, Detail of main-chain interactions among strands β1, β2, β3 and β26.

site compromises both the assembly of LptD and transport of LPS. Consistent with these observations, the residues Ser 531, Asn 534 and Ser 538 in L8 of LptD form hydrogen bonds with the residues Glu 139, Ser 125, Arg 150 of LptE, respectively, in the LptD–LptE complex (Fig. 4b). Previous studies showed that both *lptD4213* (LptD Δ330–352)[23] and *lptD208* (LptD Δ335–359) are defective in membrane permeability. Indeed, both deletion regions are located in L4 loop of LptD and each deletion would cause the loss of at least three hydrogen bonds between LptD and LptE (Fig. 4b). Furthermore, as L4 contributes substantially in occluding the lumen of the LptD–LptE complex, deletion of these residues would cause an opening of the barrel lumen to the extracellular side, which might be deleterious to the bacteria (Fig. 1c). In ref. 21 it was shown that *lptE14* (an LptE variant that contains multiple point mutations, including R24H, N53K, D64F, I101T, K136N and R186C) caused poor plugging of the LptD β-barrel. Based on the LptD–LptE complex structure, *lptE14* contains at least two fewer hydrogen bonds to LptD due to a single point mutation, R24H (Fig. 4c).

On the basis of the structure of the LptD–LptE complex, we propose that the hydrophobic moiety and hydrophilic portion of LPS may enter into the lipid phase and the hydrophilic LptD barrel, respectively, upon leaving LptD_NT, and the whole molecule is inserted into the outer leaflet of the outer membrane via the potential LPS exit portal (Extended Data Fig. 9). Such movement between the outer membrane bilayer and β-barrel lumen has been described in several systems[24], including

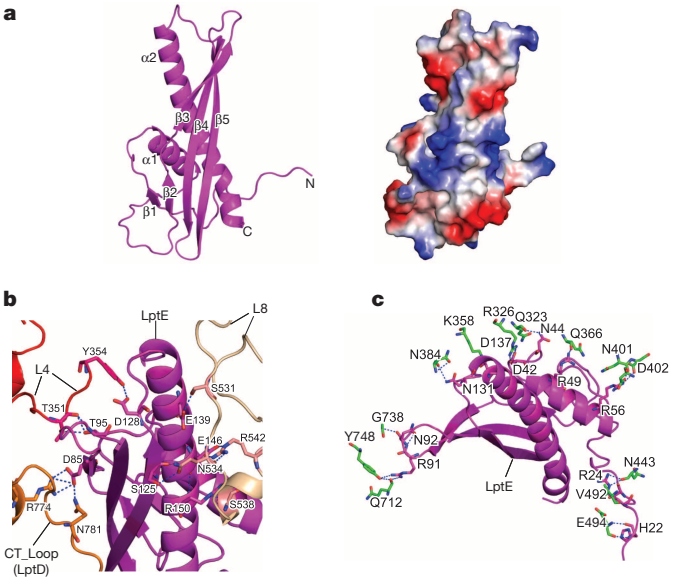

Figure 4 | Structure of LptE and its interactions with LptD. **a**, Cartoon (left) and electrostatic surface representation (right) of LptE. **b**, Detailed interactions between LptE and residues from loops of LptD. Residues from loops L4 and L8 form numerous hydrogen bonds with LptE. D85 from LptE forms a salt-bridge and a hydrogen bond with R774 and N781 of the CT_loop of LptD, respectively. **c**, Detailed interactions between LptE and residues from the barrel wall of LptD. Apart from a cluster of hydrogen bonds, residues D42, D137 and R56 of LptE form salt-bridge interactions with residues R326, K358 and D402, respectively.

some long-chain fatty acid transporter FadL, the small outer membrane proteins OmpW and OprG, and the acyltransferase PagP[25]. Intriguingly, the lateral openings of PagP are flanked by proline residues that interrupt hydrogen bonding between neighbouring β-strands, and this strategy may also be used by LptD during outer membrane insertion of LPS.

Because LPS export and outer membrane insertion are essential for bacterial viability under most conditions, this process represents an excellent drug target against pathogenic bacteria. A group of peptidomimetic compounds based on the structure of protegrin I have been shown to target LptD, and a lead compound is active against the opportunistic pathogen *Pseudomonas aeruginosa*[16]. The crystal structure of the LptD–LptE complex will open an avenue to new antibiotic strategies targeting the bacterial outer membrane.

METHODS SUMMARY

We cloned *LptD* and *LptE* genes from *S. flexneri* genomic DNA as well as their respective homologues from twelve other Gram-negative species. The *LptD* gene and its cognate *LptE* gene were subcloned into the tightly controlled expression vector pBAD22 for co-expression. Of the thirteen LptD–LptE homologues, only three complexes were successfully overexpressed and purified. We focused on the LptD–LptE complex from *S. flexneri*, which gave a relatively higher yield and has three-residue and one-residue difference in LptD and LptE, respectively, to the functionally well-characterized LptD–LptE complex from *E. coli*. Native and selenomethionine-substituted LptD–LptE complex were crystallized in space group $C2$ and $C222_1$, respectively. The structure was first solved with the single-wavelength anomalous dispersion (SAD) method in the selenomethionine-derivative crystal form, and then it was solved using the molecular replacement and refined at 2.4 Å resolution using native data set. The crystallographic statistics are listed in Extended Data Table 1.

Online Content Methods, along with any additional Extended Data display items and Source Data, are available in the online version of the paper; references unique to these sections appear only in the online paper.

Received 11 April; accepted 15 May 2014.
Published online 18 June 2014.

1. Muhlradt, P. F. & Golecki, J. R. Asymmetrical distribution and artifactual reorientation of lipopolysaccharide in the outer membrane bilayer of *Salmonella typhimurium*. *Eur. J. Biochem.* **51,** 343–352 (1975).

2. Villa, R. *et al.* The *Escherichia coli* Lpt transenvelope protein complex for lipopolysaccharide export is assembled via conserved structurally homologous domains. *J. Bacteriol.* **195,** 1100–1108 (2013).
3. Bos, M. P., Tefsen, B., Geurtsen, J. & Tommassen, J. Identification of an outer membrane protein required for the transport of lipopolysaccharide to the bacterial cell surface. *Proc. Natl Acad. Sci. USA* **101,** 9417–9422 (2004).
4. Wu, T. *et al.* Identification of a protein complex that assembles lipopolysaccharide in the outer membrane of *Escherichia coli. Proc. Natl Acad. Sci. USA* **103,** 11754–11759 (2006).
5. Nikaido, H. Molecular basis of bacterial outer membrane permeability revisited. *Microbiol. Mol. Biol. Rev.* **67,** 593–656 (2003).
6. Miller, S. I., Ernst, R. K. & Bader, M. W. LPS, TLR4 and infectious disease diversity. *Nature Rev. Microbiol.* **3,** 36–46 (2005).
7. Ruiz, N., Kahne, D. & Silhavy, T. J. Transport of lipopolysaccharide across the cell envelope: the long road of discovery. *Nature Rev. Microbiol.* **7,** 677–683 (2009).
8. Ruiz, N., Gronenberg, L. S., Kahne, D. & Silhavy, T. J. Identification of two inner-membrane proteins required for the transport of lipopolysaccharide to the outer membrane of *Escherichia coli. Proc. Natl Acad. Sci. USA* **105,** 5537–5542 (2008).
9. Sperandeo, P. *et al.* Functional analysis of the protein machinery required for transport of lipopolysaccharide to the outer membrane of *Escherichia coli. J. Bacteriol.* **190,** 4460–4469 (2008).
10. Okuda, S., Freinkman, E. & Kahne, D. Cytoplasmic ATP hydrolysis powers transport of lipopolysaccharide across the periplasm in *E. coli. Science* **338,** 1214–1217 (2012).
11. Ruiz, N., Chng, S. S., Hiniker, A., Kahne, D. & Silhavy, T. J. Nonconsecutive disulfide bond formation in an essential integral outer membrane protein. *Proc. Natl Acad. Sci. USA* **107,** 12245–12250 (2010).
12. Chng, S. S. *et al.* Disulfide rearrangement triggered by translocon assembly controls lipopolysaccharide export. *Science* **337,** 1665–1668 (2012).
13. Denoncin, K., Vertommen, D., Paek, E. & Collet, J. F. The protein-disulfide isomerase DsbC cooperates with SurA and DsbA in the assembly of the essential beta-barrel protein LptD. *J. Biol. Chem.* **285,** 29425–29433 (2010).
14. Suits, M. D., Sperandeo, P., Deho, G., Polissi, A. & Jia, Z. Novel structure of the conserved gram-negative lipopolysaccharide transport protein A and mutagenesis analysis. *J. Mol. Biol.* **380,** 476–488 (2008).
15. Tran, A. X., Dong, C. & Whitfield, C. Structure and functional analysis of LptC, a conserved membrane protein involved in the lipopolysaccharide export pathway in *Escherichia coli. J. Biol. Chem.* **285,** 33529–33539 (2010).
16. Srinivas, N. *et al.* Peptidomimetic antibiotics target outer-membrane biogenesis in *Pseudomonas aeruginosa. Science* **327,** 1010–1013 (2010).
17. Prilipov, A., Phale, P. S., Van Gelder, P., Rosenbusch, J. P. & Koebnik, R. Coupling site-directed mutagenesis with high-level expression: large scale production of mutant porins from *E. coli. FEMS Microbiol. Lett.* **163,** 65–72 (1998).
18. Park, B. S. *et al.* The structural basis of lipopolysaccharide recognition by the TLR4-MD-2 complex. *Nature* **458,** 1191–1195 (2009).
19. Chimalakonda, G. *et al.* Lipoprotein LptE is required for the assembly of LptD by the beta-barrel assembly machine in the outer membrane of *Escherichia coli. Proc. Natl Acad. Sci. USA* **108,** 2492–2497 (2011).
20. Chng, S. S., Ruiz, N., Chimalakonda, G., Silhavy, T. J. & Kahne, D. Characterization of the two-protein complex in *Escherichia coli* responsible for lipopolysaccharide assembly at the outer membrane. *Proc. Natl Acad. Sci. USA* **107,** 5363–5368 (2010).
21. Grabowicz, M., Yeh, J. & Silhavy, T. J. Dominant negative lptE mutation that supports a role for LptE as a plug in the LptD barrel. *J. Bacteriol.* **195,** 1327–1334 (2013).
22. Freinkman, E., Chng, S. S. & Kahne, D. The complex that inserts lipopolysaccharide into the bacterial outer membrane forms a two-protein plug-and-barrel. *Proc. Natl Acad. Sci. USA* **108,** 2486–2491 (2011).
23. Braun, M. & Silhavy, T. J. Imp/OstA is required for cell envelope biogenesis in *Escherichia coli. Mol. Microbiol.* **45,** 1289–1302 (2002).
24. van den Berg, B. Going forward laterally: transmembrane passage of hydrophobic molecules through protein channel walls. *ChemBioChem* **11,** 1339–1343 (2010).
25. Khan, M. A. & Bishop, R. E. Molecular mechanism for lateral lipid diffusion between the outer membrane external leaflet and a beta-barrel hydrocarbon ruler. *Biochemistry* **48,** 9745–9756 (2009).

Acknowledgements The authors thank Y. Shan for discussions, H. Wu, J. Deisenhofer, Y. Jiang, N. Huang, Z. Zhou, G. Li, Z. Liu and members of the Huang group for critically reading the manuscript. The diffraction data were collected at the Shanghai Synchrotron Radiation Facility (SSRF, China) and Beijing Synchrotron Radiation Facility of China (BSRF, China). This work was supported by grants from the Ministry of Science and Technology (2012CB917302 and 2013CB910603 to Y.H.), the Strategic Priority Research Program of the Chinese Academy of Sciences (XDB080203 to Y.H. and X.C.Z.) and the National Natural Science Foundation of China (31170698 to Y.H.).

Author Contributions Y.H. supervised the project. S.Q. and Q.L. performed the experiments. S.Q., Y.Z. and Y.H. collected diffraction data. Y.H. built the model and refined the structure. Y.H., X.C.Z., S.Q. and Y.Z. contributed to manuscript preparation. Y.H. wrote the manuscript. All authors contributed to data analysis. Correspondence and material request should be address to Yihua Huang. The authors declare no competing financial interests.

Author Information The coordinates and diffraction data of the LptD–LptE complex crystal structure have been deposited in the Protein Data Bank with the accession code 4Q35. Reprints and permissions information is available at www.nature.com/reprints. The authors declare no competing financial interests. Readers are welcome to comment on the online version of the paper. Correspondence and requests for materials should be addressed to Y.H. (yihuahuang@sun5.ibp.ac.cn).

METHODS

Protein expression, purification and crystallization. The *LptD* and *LptE* genes (including signal peptide coding sequence) were obtained from the genomic DNA of *S. flexneri* and 12 other Gram-negative bacterial species (American Type Culture Collection) using a standard PCR protocol. The PCR products were then subcloned into pRSFDuet-1 (Novagen) with endonuclease restriction enzymes NcoI/HindIII for LptD, and NdeI/XhoI for LptE, respectively. The generated plasmid pRSFDuet-1-*LptD–LptE* contained a hexahistidine tag at the C terminus of LptE that was introduced in the PCR primer to facilitate subsequent affinity purification. To achieve high protein expression levels, the *LptD-T7-rbs-LptE* sequence in the pRSFDuet-1-*LptD–LptE* plasmid was excised and further ligated into a modified pBAD22 vector via restriction enzymes NcoI/XhoI, followed by removal of the *T7* promoter preceding to LptE sequence using overlap PCR. The constructed plasmid pBAD22-LptD–LptE was then transformed into *E. coli* BL21 (DE3) omp8 cells[17] for co-expression of LptD and LptE. Protein expression was induced by the addition of 0.4% L-arabinose for 10 h at 26 °C when the $OD_{600\,nm}$ of the culture reached about 2.0. Cells were subsequently collected by centrifugation at 4,500*g* for 30 min at 4 °C. Cell pellets were resuspended in 1 × PBS (pH 7.4), lysed by a single passage through a French Press (JN-3000 PLUS, China) at 16,000 p.s.i., and centrifuged at 39,000*g* for 1 h at 4 °C to collect the total cell membranes. To remove inner membranes, the total membranes were further solubilized with a buffer containing 1 × PBS (pH 6.9) and 1% *N*-lauroylsarcosine sodium (Sigma-Aldrich) for 1 h at 4 °C. The outer membranes were isolated by centrifugation at 39,000*g* for 1 h at 4 °C and were solubilized for 1 h with buffer 1 (20 mM Tris-HCl (pH 8.0), 300 mM NaCl, 20 mM imidazole and 1% (w/v) *N*,*N*-dimethyldodecylamine *N*-oxide (LDAO)). The supernatant was collected after centrifugation at 39,000*g* for 1 h at 4 °C and incubated with pre-equilibrated Ni-NTA agarose beads for 1 h at 4 °C. Ni-NTA agarose beads were rinsed with buffer 1 and buffer 2 (20 mM Tris-HCl (pH 8.0), 150 mM NaCl, 30 mM imidazole and 0.2% LDAO), and detergent exchange was performed with buffer 3 (20 mM Tris-HCl (pH 8.0), 150 mM NaCl, and 1% (w/v) tetraethylene glycol monooctyl ether (C_8E_4)). LptD–LptE complex was eluted from the Ni-NTA agarose beads using buffer 4 (20 mM Tris-HCl (pH 8.0), 150 mM NaCl, 200 mM imidazole and 1% C_8E_4). The eluted LptD–LptE complex was concentrated and subsequently applied to a Resource-Q column (GE Healthcare), and followed by a Superdex 200 10/300 size exclusion column (GE Healthcare) that was pre-equilibrated with 20 mM Tris-HCl (pH 8.0), 150 mM NaCl and 0.6% C_8E_4. The peak fractions were pooled and concentrated to approximately 10 mg ml^{-1}.

Crystallization was conducted at 16 °C using the hanging drop vapour diffusion method by mixing the protein and precipitants at a ratio of 1:1. Crystals of the LptD–LptE complex appeared in a buffer containing 100 mM sodium citrate (pH 5.6), 300 mM lithium sulphate, 8% (v/v) PEG400 and 100 mM glycine overnight, and grew to their final size in approximately one week. SeMet-substituted crystals were obtained in a crystallization condition that contains 100 mM sodium citrate (pH 5.6), 400 mM lithium sulphate and 8% PEG400 with 10 mM TCEP as additive.

Structure determination and refinement. Diffraction data were collected at Shanghai Synchrotron Radiation Facility (SSRF, Shanghai, China) and processed with HKL2000[26]. The heavy atom search and initial phase determination were performed with AutoSol from PHENIX[27] package using the SeMet-LptD–LptE data set at 3.5 Å. Cα chains of LptD–LptE were partially built using AutoBuild[27] and further extended manually using the 3.5 Å map generated from AutoSol[27]. A high resolution map at 2.4 Å of the native-LptD–LptE data set was obtained by molecular replacement using the program PHASER[27] and the Cα chain built from the SeMet data set as a search model. Density modification and auto model building of the native-LptD–LptE map were further performed using AutoBuild. The initial output model (~70% completeness) from Autobuild was then manually corrected and completed with COOT[28]. Refinements of the native-LptD–LptE data set were performed using PHENIX and CCP4[29]. All structure figures were rendered using PyMOL[30]. The refinement statistics are listed in Extended Data Table 1.

26. Otwinowski, Z. & Minor, W. Processing of X-ray diffraction data collected in oscillation mode. *Methods Enzymol.* **276,** 307–326 (1997).
27. Adams, P. D. *et al.* PHENIX: building new software for automated crystallographic structure determination. *Acta Crystallogr. D* **58,** 1948–1954 (2002).
28. Emsley, P. & Cowtan, K. Coot: model-building tools for molecular graphics. *Acta Crystallogr. D* **60,** 2126–2132 (2004).
29. Collaborative Computational Project, number 4. The CCP4 suite: programs for protein crystallography. *Acta Crystallogr. D* **50,** 760–763 (1994).
30. DeLano, W. L. PyMOL molecular viewer: Updates and refinements. *The 238th ACS National Meeting* **238** (2009).

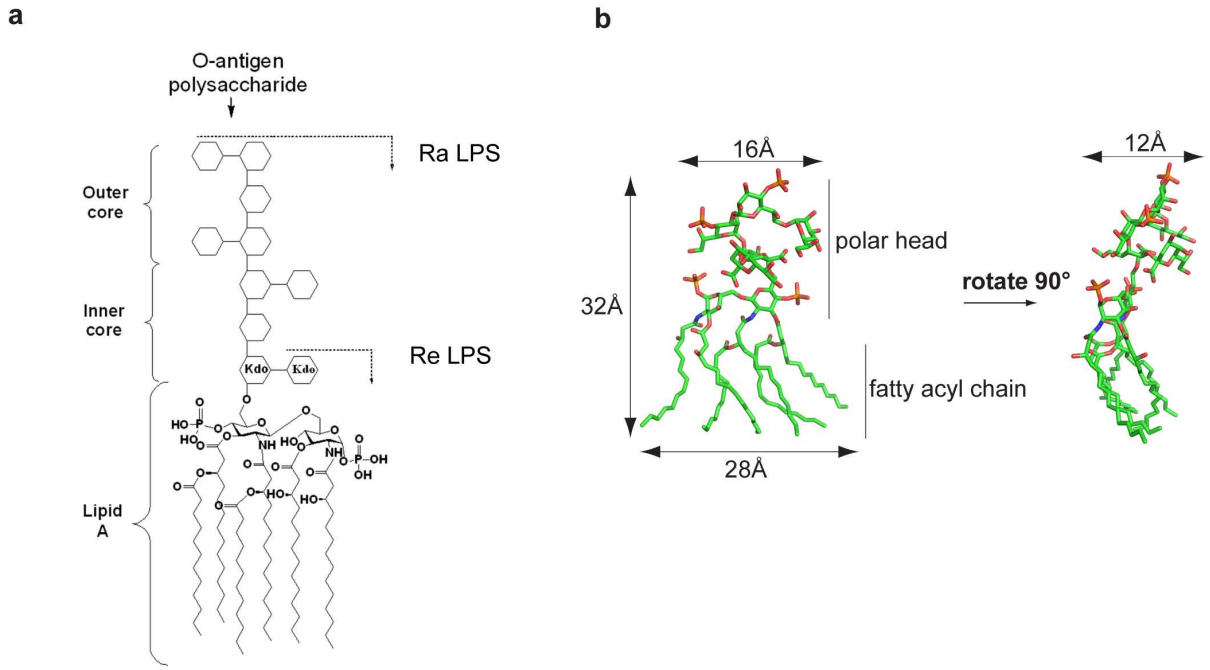

Extended Data Figure 1 | Chemical structure and dimensions of LPS. **a**, Chemical structure of LPS. LPS is composed of three modules: lipid A, a core oligosaccharide and a highly variable O-antigen constituted of repeating oligosaccharide units. The core is covalently linked to lipid A and can be further divided into inner and outer core. The inner core contains at least one residue of 3-deoxy-D-manno-oct-2 ulosonic acid (Kdo) linking to lipid A. **b**, Ra LPS is about 32 Å in height and 28 Å × 12 Å in the other two dimensions. The size of Ra LPS is based on the crystal structure of the TLR4/MD-2/Ra LPS complex (PDB ID 3FXI).

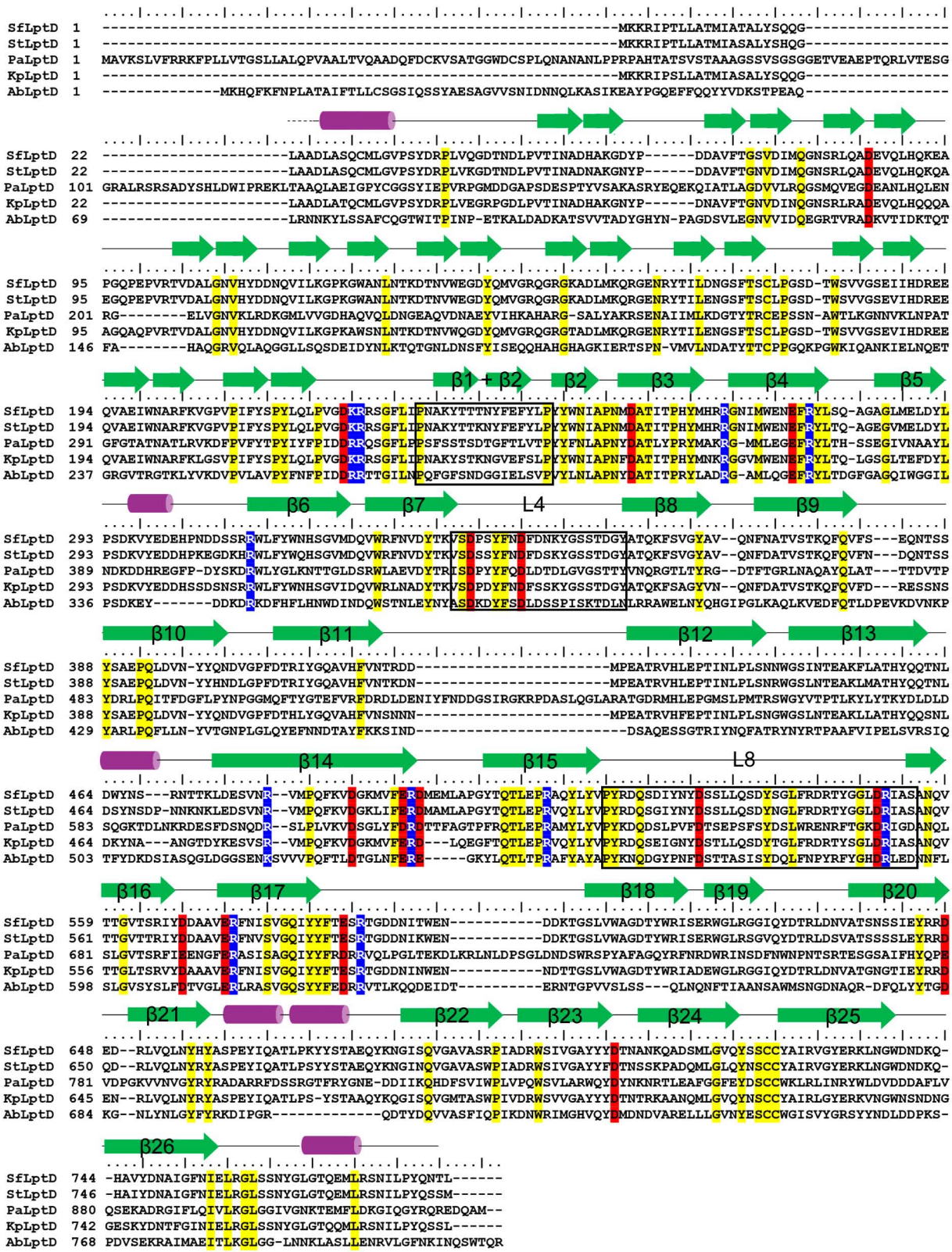

Extended Data Figure 2 | Sequence alignment of LptD proteins from five representative Gram-negative bacterial species. Secondary structures of LptD from *S. flexneri* (SfLptD) are labelled at the top of the sequence alignment. Strands that consist of the β-barrel of LptD are numbered. Residues of the two distorted β-strands (β1 and β2), L4 and L8 are boxed. Identical hydrophobic residues, positively-charged residues and negatively-charged residues are highlighted in yellow, blue and red, respectively. Three proline residues Pro 231, Pro 246 and Pro 261 in SfLptD are conserved in different species. SfLptD, StLptD, PaLptD, KpLptD and AbLptD represent LtpD sequences from *S. flexneri, Salmonella enteric* Typhimurium str. LT2, *P. aeruginosa*, *Klebsiella pneumoniae* and *Acinetobacter baumannii*, respectively.

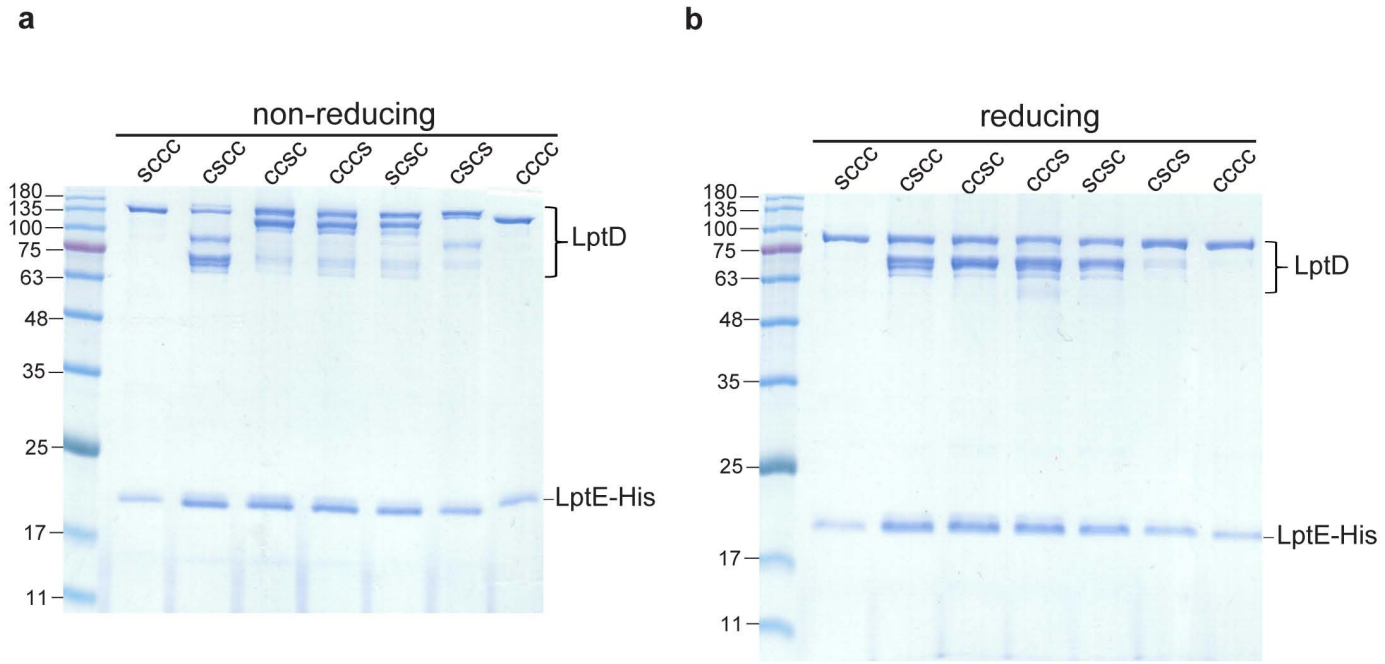

Extended Data Figure 3 | Two pairs of disulphide bonds are important for the stability and folding of LptD. **a**, Non-reducing SDS–PAGE showing the purified LptD mutant proteins containing different Cys-to-Ser mutations. CCCC indicates that amino acids present at positions 31, 173, 724 and 725 in LptD are cysteine residues. LptD with mutation to Ser at different positions in the LptD sequence are co-expressed with LptE–His. **b**, Reducing SDS–PAGE showing LptD mutant proteins containing different Cys-to-Ser mutations. Samples were reduced by addition of 10 mM β-mercaptoethanol in the SDS–PAGE loading dye. All samples were boiled for 10 min at 95 °C. The degradation bands that appear below wild-type LptD were confirmed to be LptD fragments by mass spectrometry. All data shown are representative of at least three independent experiments.

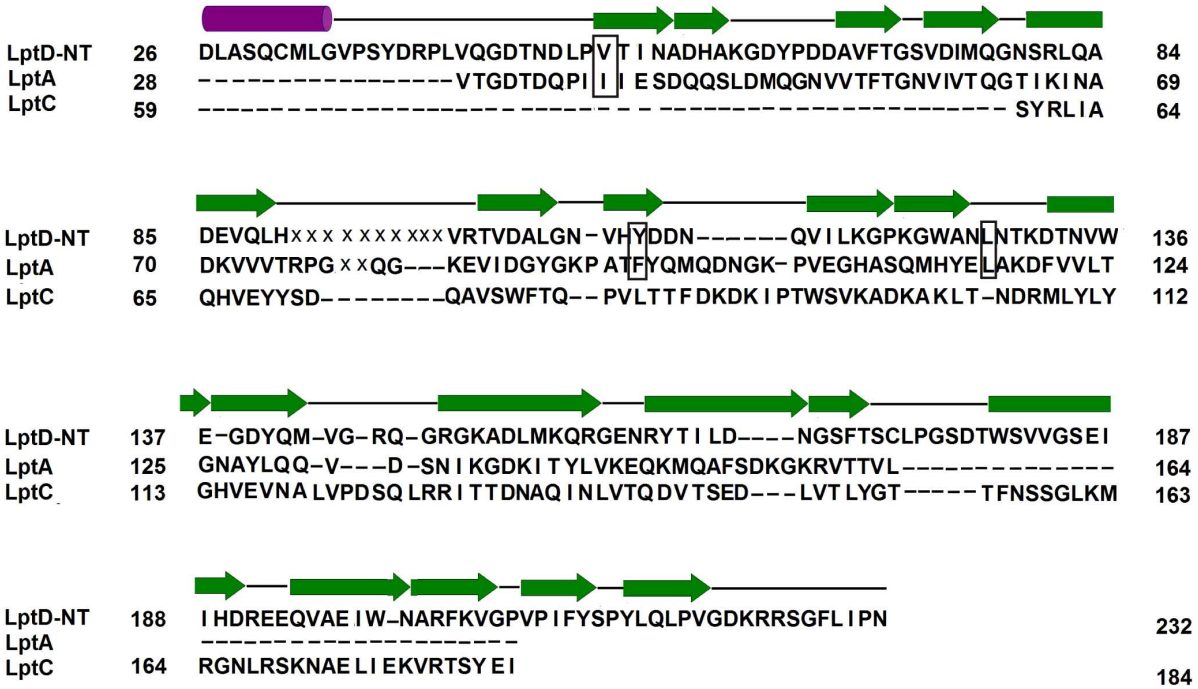

Extended Data Figure 4 | Structure-based sequence alignment of LptD_NT with LptA and LptC. The three sequences show very low sequence identity, but have similar secondary structures and folds. The three LPS-binding residues in LptA and LptD_NT are boxed ('×' indicates residues that are invisible in the crystal structure).

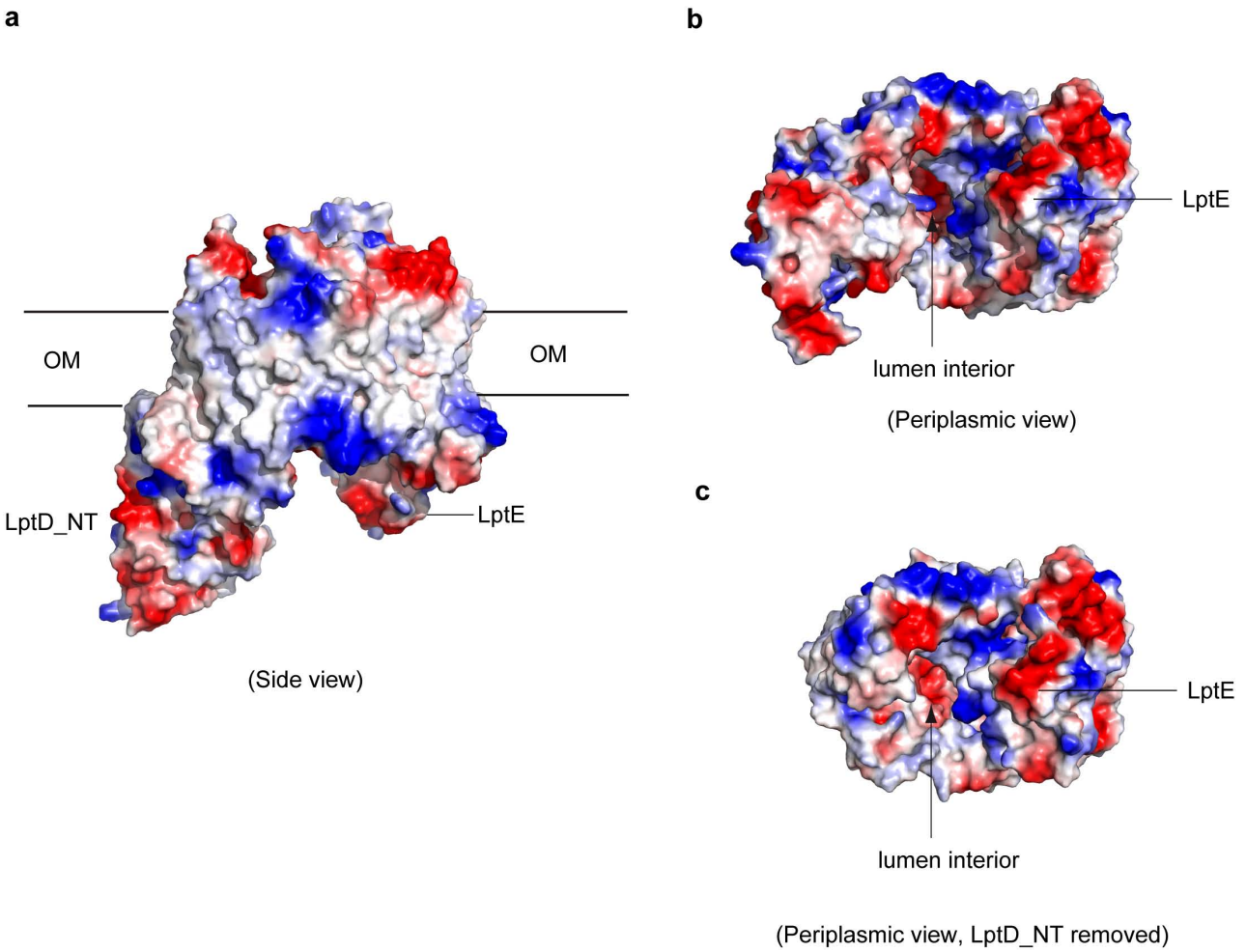

Extended Data Figure 5 | Electrostatic potential representation of the LptD–LptE complex. **a**, Electrostatic surface of the LptD–LptE complex (side view). The hydrophobic girdle indicates the membrane-bound region, and this was verified by the presence of the expected aromatic belts. **b**, **c**, Periplasmic view of the interior surface properties of LptD–LptE complex (**b**) and that of LptD–LptE complex with LptD_NT domain removed (**c**). The interior surface of the complex is fairly hydrophilic with evenly distributed hydrophobic and hydrophilic residues lining inside.

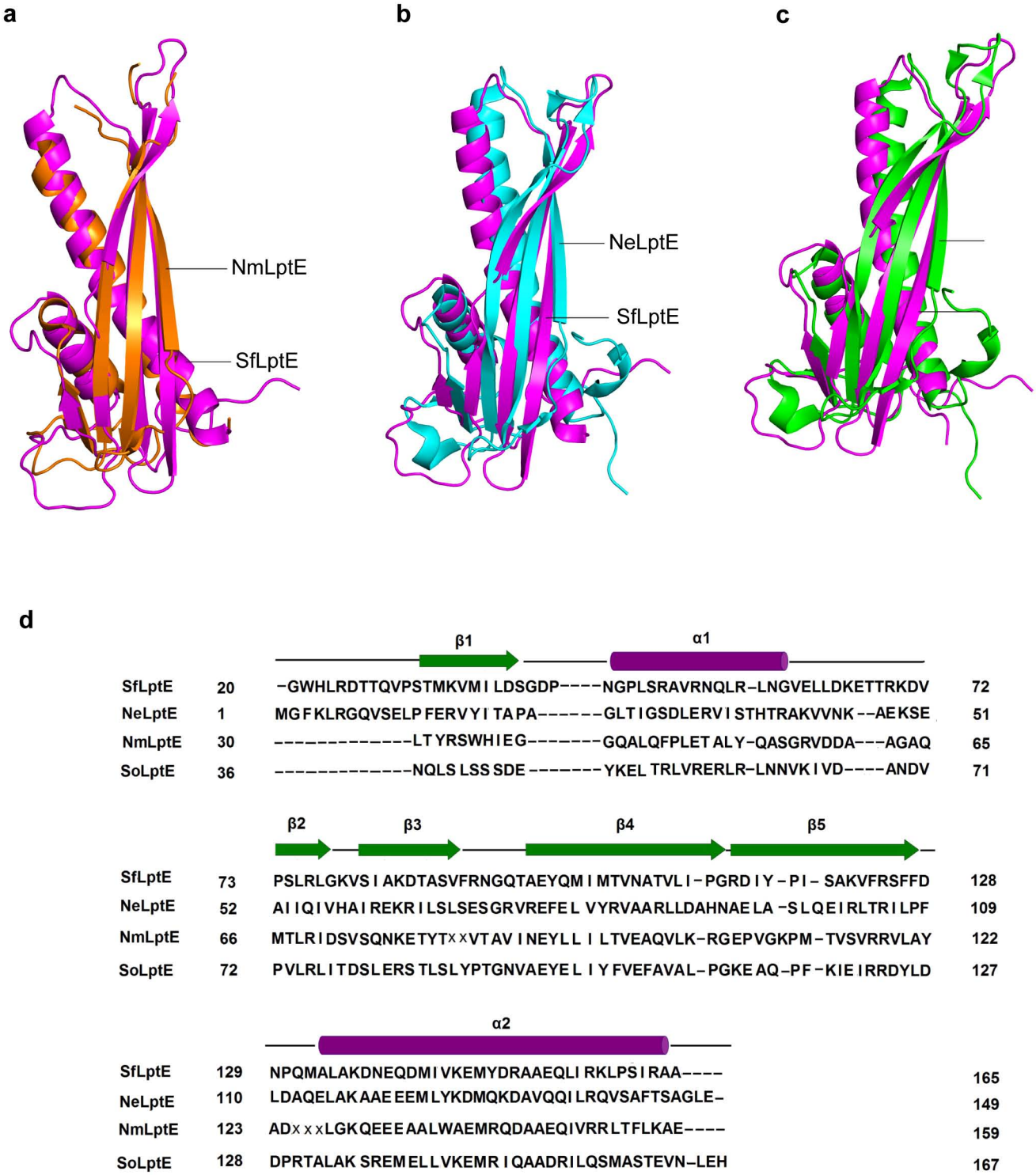

Extended Data Figure 6 | Structure superposition and sequence alignment of LptE orthologues. **a**–**c**, Superposition of SfLptE with NmLptE (**a**), NeLptE (**b**) and SoLptE (**c**). **d**, Structure-based sequence alignment of SfLptE with NeLptE, NmLptE and SoLptE. SfLptD, NmLptE, NeLptE and SoLptE are coloured in magenta, orange, cyan and green, respectively. SfLptE, NeLptE, NmLptE and SoLptE represent LptE orthologues from *S. flexneri*, *N. europaea*, *N. meningitides* and *S. oneidensis*, respectively. Secondary structure elements are labelled on the top. The primary structures of these LptE orthologues have very low sequence identity, but their secondary structure distribution and fold are quite similar.

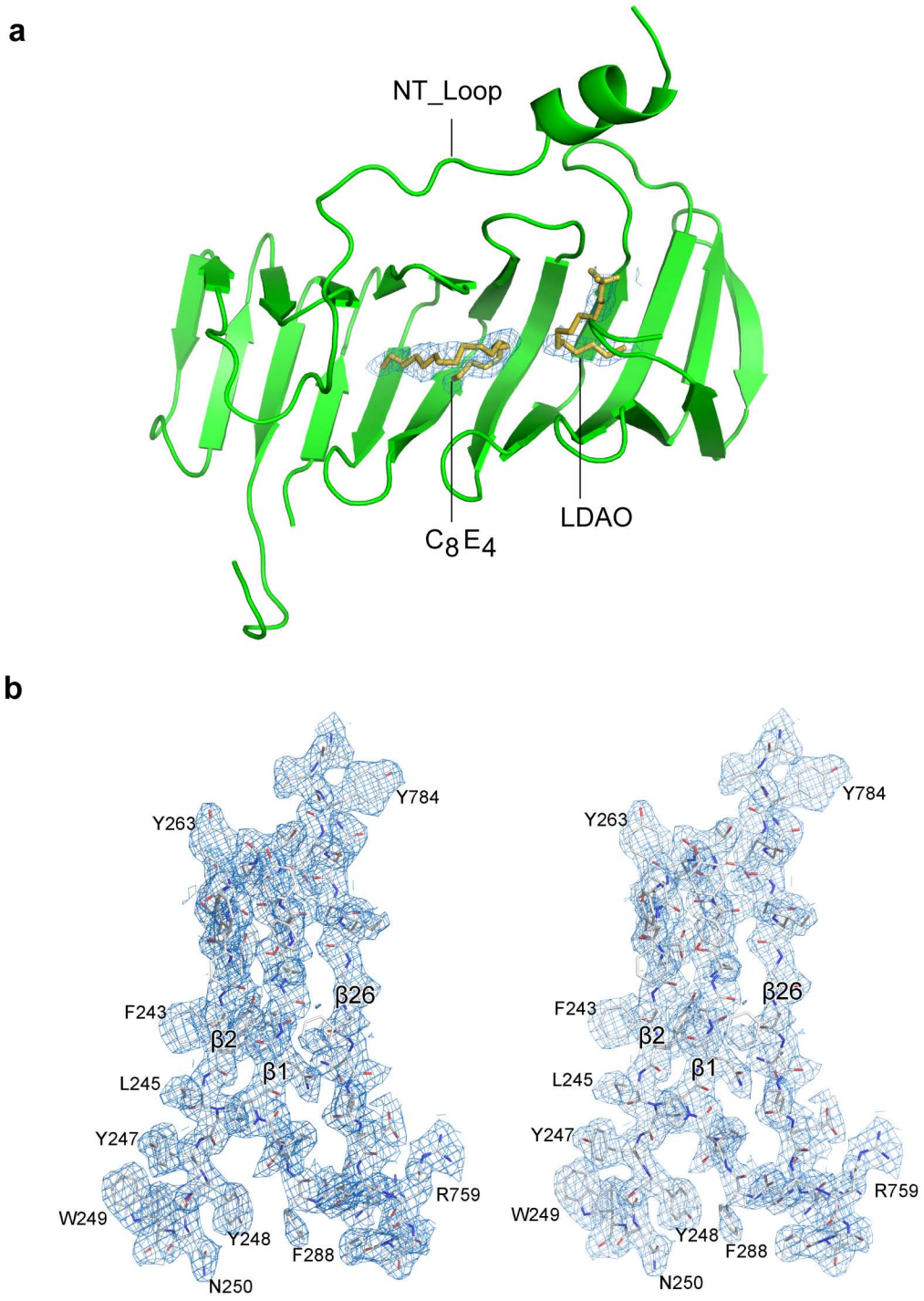

Extended Data Figure 7 | Electron density maps showing detergent molecules in the LptD_NT groove and residues at the LPS exit portal. **a**, Electron density maps ($2F_o - F_c$) showing the presence of two detergent molecules in the groove of LptD_NT. **b**, Stereo view of electron density map ($2F_o - F_c$) of residues at the potential LPS exit portal. The contour level for maps is 1.0σ.

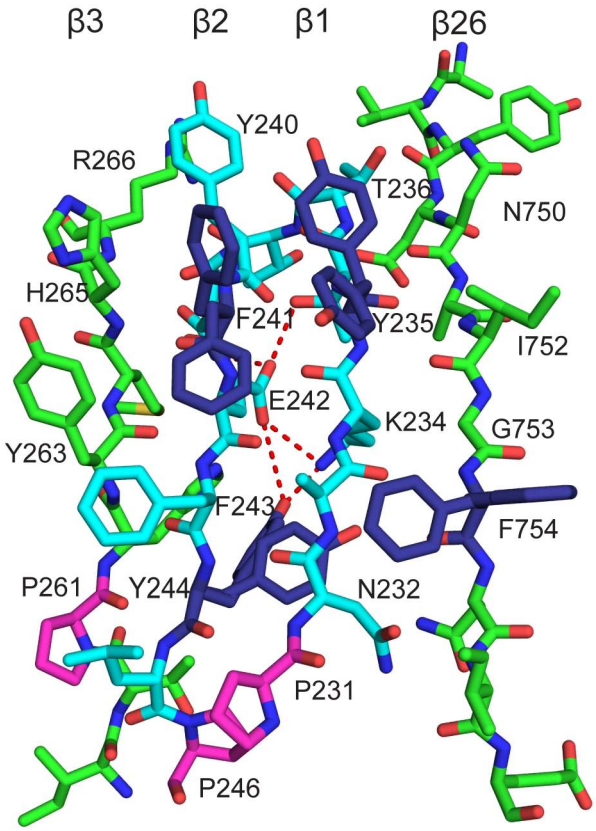

Extended Data Figure 8 | Residue E242 of LptD forms a polar-interaction network within strands β1 and β2. Residue E242 of LptD forms a salt-bridge interaction with K234 and a few hydrogen bonds with residues of strands β1 and β2.

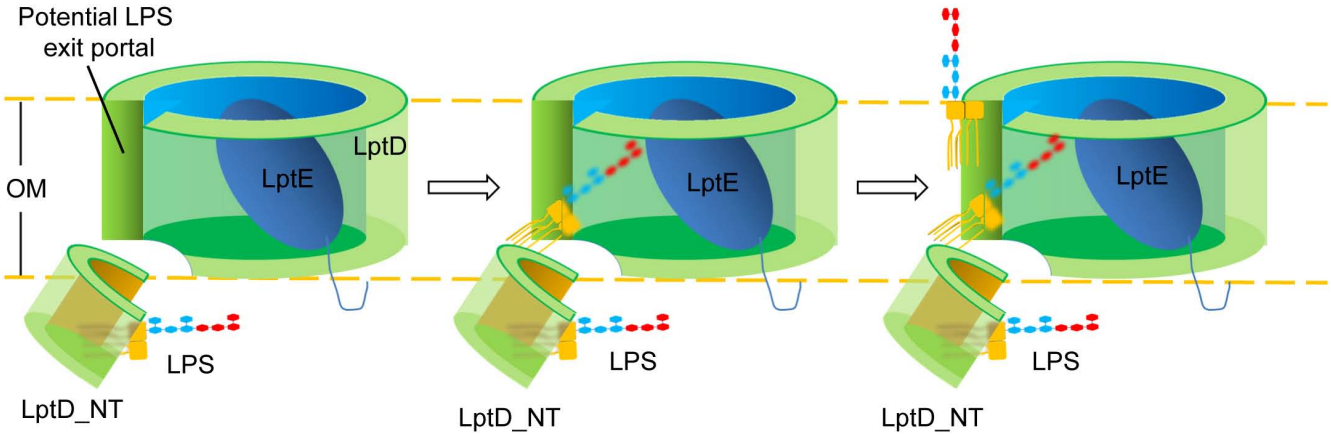

Extended Data Figure 9 | Proposed model for LPS insertion into bacterial outer membrane. LptD_NT relays LPS from LptA. Portion of LptD_NT of LptD likely resides in the outer membrane, and the LPS-conduit of the β-jellyroll is open to lipid phase (Fig. 1c). At the interface of LptD_NT domain and the β-barrel of LptD, the hydrophobic portion of LPS may directly enter into the lipid phase, whereas the hydrophilic moiety of LPS may enter into the barrel of LptD. The LPS molecules are inserted into the outer leaflet of the outer membrane upon dislocation of strands β1 and β2. LptE is a lipoprotein, and probably binds to the hydrophilic head groups of LPS in the process.

Extended Data Table 1 | Data collection and refinement statistics

Statistics	Values	
Data collection		
Protein crystal	Native	SeMet
Beamline	BL17U	BL17U
Wavelength (Å)	0.97906	0.97923
Space group	C2	$C222_1$
Cell dimensions		
a, *b*, *c* (Å)	240.8, 116.6, 68.0	96.7, 234.4, 226.3
α, β, γ (°)	90.0, 103.7, 90.0	90.0, 90.0, 90.0
Resolution (Å)	50-2.4	50-3.4
R_{sym} (%)	12.4 (>100)	15.2 (>100)
Completeness (%)	99.7 (99.6)	99.5 (98.8)
$I/\sigma(I)$	13.6 (3.8)	15.2 (3.4)
Unique reflections (*n*)	71,148 (7,116)	35,758 (3,508)
Redundancy	11.9 (11.7)	11.3(11.1)
Refinement		
Resolution (Å)	50-2.4	
Reflections (*n*)	71,127 (3,666)	
R_{work}/R_{free} (%)[a]	18.6/23.0	
Number of atoms (*n*)		
Protein	7,379	
Detergent	213	
Solvent	573	
B-factor ($Å^2$)		
Protein	31.8	
Detergent	54.2	
Solvent	36.2	
Molprobity clashscore	5.26	
RMSD		
Bond length (Å)	0.007	
Bond angles (°)	1.256	
Ramachandran plot (%)		
Most favored	96.9	
Allowed	3.1	

Values in parentheses refer to the highest resolution shell.
[a]R_{free} was computed as for R_{work} using a 5% test set of randomly selected reflections that were omitted from the refinement.